Eksplorium
Volume 43 No. 1, May 2022: 41–58

p-ISSN 0854-1418
e-ISSN 2503-426X

Geostatistical Ore Body Modeling on Uranium Mineralization in Remaja Sector, Kalan Area, West Kalimantan

Roni Cahya Ciputra[1,2]*, Mohamad Nur Heriawan[1], Heri Syaeful[2], Dhatu Kamajati[3], Putri Rahmawati[3]
[1]Faculty of Mining and Petroleum Engineering, Bandung Institute of Technology (ITB)
Ganesha St., No. 10, Bandung 40132, Indonesia
[2]Research Center for Nuclear Fuel Cycle and Radioactive Waste Technology,
Research Organization for Nuclear Energy (ORTN), National Research and Innovation Agency (BRIN)
PUSPIPTEK Area, Building 20, South Tangerang 15314, Indonesia
[3]Bureau for Public Communication, General Affairs, and Secretariat,
National Research and Innovation Agency (BRIN)
B.J. Habibie Building, M.H. Thamrin St., No. 8, Central Jakarta 10340, Indonesia
*E-mail: roni.cahya.ciputra@brin.go.id

Article received: 18 May 2022, revised: 24 May 2022, accepted: 31 May 2022
DOI: 10.17146/eksplorium.2022.43.1.6622

ABSTRACT

Manual ore body modeling on Remaja Sector, Kalan, West Kalimantan generally takes a long time and is subjective. On the other hand, automatic modeling (implicit modeling) is faster, objective, and equipped with uncertainty factors. This study aimed to analyze the comparison between the geostatistical Sequential Indicator Simulation (SIS) ore body model to the manual ore body model. The lithology database was used as input for variogram analysis and SIS simulation. The directional variogram was used to construct an experimental variogram for the lithology with orientation data. The orientation of the lithologies corresponds to the anisotropy of their variogram map. The SIS was carried out in Block A and Block B with block sizes of 6×6×6 m^3 and 5×5×5 m^3 respectively. The simulation results were processed to produce a lithology probability model. By using maximum probability as block lithology, simulation results were well validated by the composite database histogram, the lithologies along the tunnel on the geological map of level 450 masl of Eko Remaja Tunnel., and the lithologies along boreholes. The weakness of the geostatistical ore body model was the results depending on the input parameters. Meanwhile, several advantages of the geostatistical ore body model were a faster processing process, equipped with an uncertainty factor, and the block size of the model has taken into account the distance between grade data so that it can be used directly for grade estimation. Quantitatively, the geostatistical ore body model had a higher average percentage of conformity to the lithology of the mineralized zone along the borehole than the manual ore body model.

Keywords: Kalan, geological modeling, geostatistics, sequential indicator simulation, uranium

INTRODUCTION

Kalan, located in the northern area of the Schwaner Mountains at Melawi Regency (Figure 1), West Kalimantan is a target area for Indonesia's uranium exploration project since 1969 with uranium resources [1]–[4]. As the nuclear power plant became one of the research topics in the 2020-2024 national priority research document, uranium supply for nuclear fuel raw material became one of the critical derivative topics for research. Remaja Sector which has the most data among other uranium sectors in Kalan is considered important for resources re-evaluation with the current method and economical background after a feasibility study in 1991 stated that it was not feasible.

However, there are still some problems in the evaluation. The ore body modeling in the Remaja Sector was done manually vein-per-vein like other resource evaluations in Kalan [5]–[7]. The manual modeling took so much time due to the complex geological situation of the sector. The model also contained subjectivity. Such problems are said to cause risk for further mining processes [8]. Another problem is the irregular data spacing between drill holes and different data intervals between lithological data and the equivalent grades.

Because of that problems, the manual model needs to be compared with another faster, more objective, and equipped with an uncertainty modeling method. It is also necessary to determine the suitable ore body block size parameter so that the resource model can be developed. This study aimed to analyze the comparison between the ore body model using the geostatistical Sequential Indicator Simulation (SIS) method to the manual ore body model.

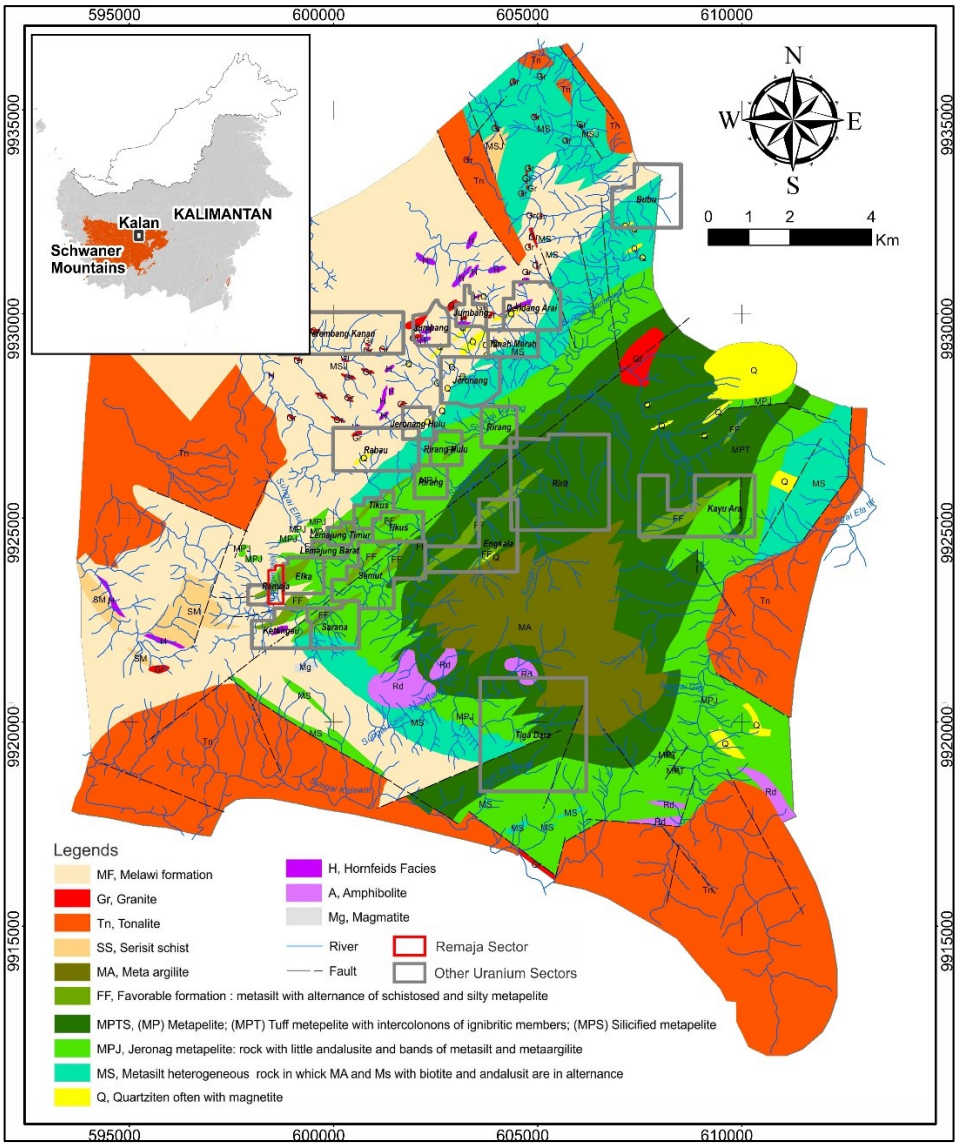

Figure 1. Regional geological map of Remaja Sector (modified from [5], [31]).

p-ISSN 0854-1418
e-ISSN 2503-426X

THEORY

Geostatistics is a part of statistics that integrates spatial continuity to model a regional variable, a function that describes the value in space [9], [10]. To measure spatial continuity, a semivariogram or variogram is used in geostatistics [9], [10] as described below:

$$\gamma(h) = \frac{1}{2N(h)} \sum_{i=1}^{N} [(z(x_i) - z(x_{i+h})]^2 \qquad (1)$$

where $\gamma(h)$ is the semivariogram or variogram, $N(h)$ is the number of data pairs that are separated by vector h, $z(x_i)$ is the sample value of point i, dan $z(x_{i+h})$ is the sample value of a point separated by vector h from point i. Variogram fitting based on the theoretical model is substantial to obtain the variogram model required for geostatistical estimation or simulation.

Indicator Kriging (IK) and Sequential Indicator Simulation (SIS) are the two types of indicator-based geostatistical methods that are most often used in geological modeling [11], [12]. The indicator-based geostatistical method means that the data used for the algorithm need to be converted to the binary format of 1 and 0. The IK method estimated a probability to obtain a minimum error, while SIS generates a series of values that has histogram and variance properties close to the input data [11], [13]–[15]. The SIS method in geological modeling is considered to improve domain definition and quantify uncertainty [14], [16]. The SIS method depends on IK to yield a probability density function (PDF) of categorical variables. With Monte Carlo simulation, the method simulated non-parametric distribution combined with the sequential indicator formalism [13], [15], [17], [18]. The method produces a series of alternative values, called realization, which shows the probability distribution of the same indicator variable. The realization may be close in value but not identical to each other [11], [19], [20]. From all the values of realization on each block, an uncertainty value of each lithology on the respective block can be determined. The uncertainty yielded from the simulation can be treated as block domain weight in resource modeling. In some geological modeling research, SIS was preferred over IK as it visualized the model closer to actual circumstances [21], [22]. Many other research using SIS manifested satisfactory models [13], [15], [16], [23], [24].

GEOLOGY OF STUDY SITE

The Remaja Sector is located in the southwestern part of the Kalan Basin. The area of this sector includes Bukit Eko in the upper reaches of the Kalan River. The basin itself is part of northern Schwaner Mountain [25], [26]). It consists of a series of metamorphic rocks belonging to Pinoh Metamorphic that intruded by younger granitoid of Sepauk Tonalite and Sukadana Granit [25]–[27]. The regional geological map of the Remaja Sector is depicted in Figure 1. The lithology of the Remaja Sector includes metasiltstone, schistose metapelite, 'Jeronang' andalusite metapelite, and metaampelite. In general, the strike and dip of the lithology (S0) are N50−90ºE/50º. The schistosity plane (S1) of schistose metapelite lithology lies N230ºE/70−80º [28]. The host rock of uranium mineralization is schistose metapelite and metasiltstone which stratigraphically lies between the uranium-sterile ‘Jeronang’ metapelite layers. Between 1982 and 1991, there was a trial underground mining project on Eko Hill of Remaja Sector after detailed exploration. The project

revealed more detail about the uranium mineralization and geology of the sector on the mining tunnel called the Eko-Remaja Tunnel. The geological map of level 450 masl of the tunnel is displayed in Figure 2.

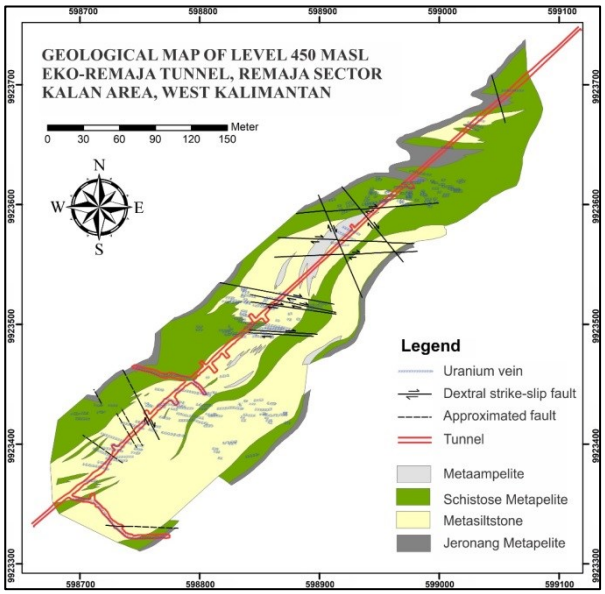

Figure 2. The geological map of the Eko-Remaja Tunnel at level 450 masl (modified from [31]).

The fracture group trending west–east facing north with a dip of 50 – 80, which is relatively parallel to the schistosity plane, is filled with uranium mineralization [29], [30]. It took place on tourmaline–purple quartz vein.

In detail, mineralized veins in this location can be divided into three types. From old to young, respectively, there are tourmaline breccia veins, tourmaline feldspar veins, and quartz-feldspar veins [28]. The first two types of veins are similar in composition and contain high levels of uranium. Meanwhile, quartz-feldspar veins contain low levels of uranium and are scattered near the sterile zone. Microthermometric studies show that the temperature for the formation of breccias and tourmaline veins is between 260–325º C, while quartz-feldspar veins are at 285º C. Chronologically, the mineralized veins in the tunnel were then cut by gypsum-calcite veins. This group of veins is formed at a lower temperature of 145º–195º C [28], [32]. Uranium minerals found in veins are uraninite, brannerite, davidite, and gummite [1], [3]. These uranium minerals are associated with pyrite, pyrrhotite, chalcopyrite, cobaltite, lollingite, pentlandite, sphalerite, molybdenite, ilmenite, magnetite, and chlorite. The appearance of mineralization can be seen in Figure 2. Age dating using U and Pb isotopes that have been carried out on uraninite from the Eko-Remaja Tunnel results in a formation period of 131–160 million years ago [33]. This is appropriate to the period of Southwest Borneo (SWB) accretion in Sundaland that forms the Pinoh Metamorphic Rock in recent studies [25], [26]. This also reinforces the concept of stratigraphic mineralization which emphasizes lithological control of mineralization in the Remaja Sector [3].

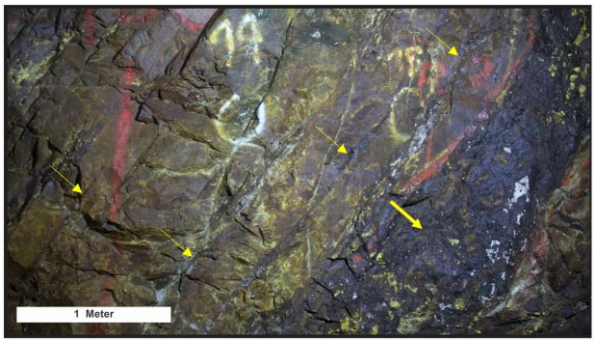

Figure 2. Uranium mineralization in tectonic breccia (thick arrow) and tourmaline veins (thin arrows) [30].

DATA AND METHOD

The research flowchart, as can be seen in Figure 3 summarized the method that has been used in this research. There were 309 borehole data in the Remaja Sector that were suitable for geostatistical analysis. These data are divided into two Block Areas, they are Block A and Block B. The data separation was done also for the sake of geostatistical suitability due to the quite far distance

p-ISSN 0854-1418
e-ISSN 2503-426X

between the two blocks area, as depicted in Figure 4. The Binary lithology database was constructed with six categorical variables with numerical code: metasiltstone or ML (0), schistose metapelite or MPS (1), 'Jeronang' metapelite or MPJ (2), metaampelite (3), microdiorite or MD (4), and mineralization zone or ZM (5). At each data point, an array of binary of 0 or 1 is assigned to the variables where 1 is only assigned for the corresponding lithology of the data point. The statistical parameter, frequency, and global proportion of each category in Block A and Block B are displayed in Table 1.

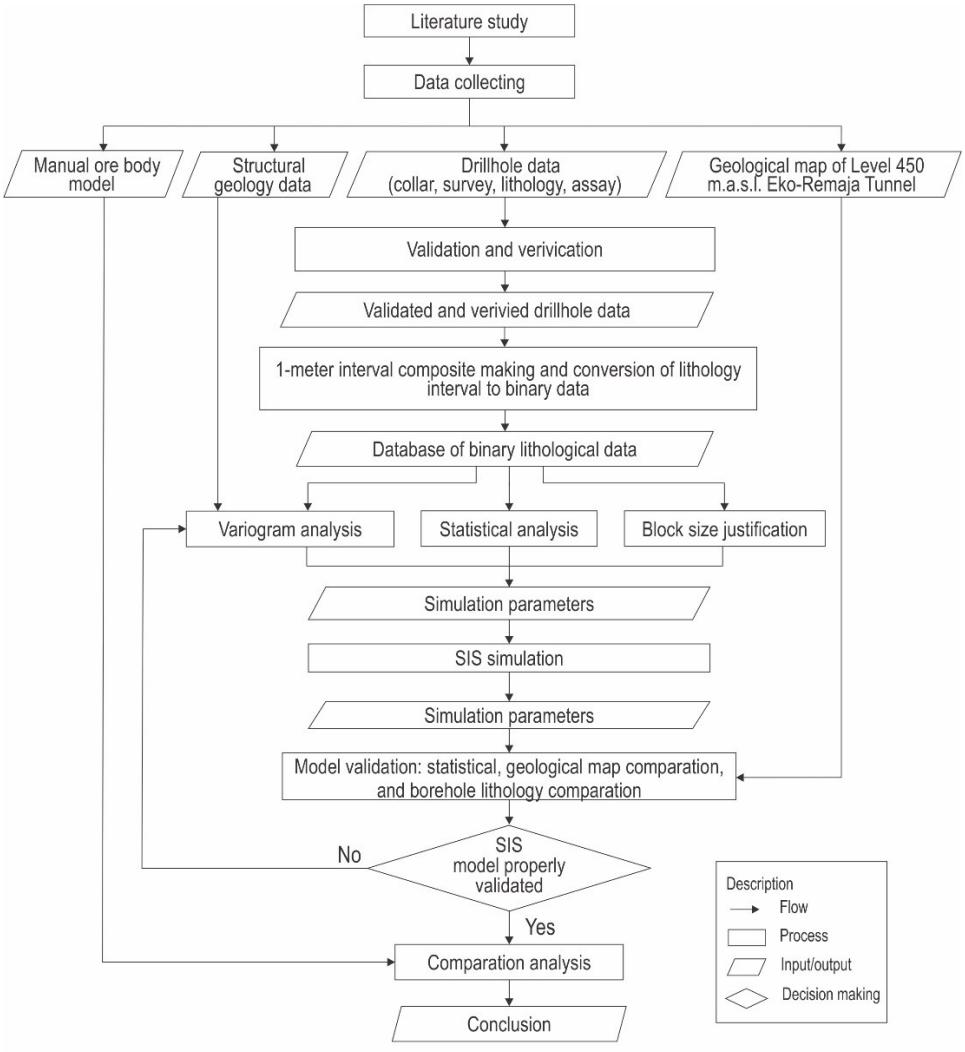

Figure 3. The research flowchart.

The data spacing of lithological data and the equivalent grades were calculated in search of the most representative block size for the ore geostatistical body model. Because the data spacing is relatively tricky in the fan-shaped borehole configuration as can be seen in Figure 4, the data spacing was calculated per interval 5-meter elevation. Based on the lithological data, the average data spacings were 10.8 m and 12.1 m respectively for Block A and Block B. Based on the eU_3O_8 grade data, the average data spacing was 10.1

m and 9.5 m respectively for Block A and Block B. The block size of 6×6×6 m^3 and 5×5×5 m^3 respectively for Block A and Block B was used for the model. These block sizes were considered appropriate to represent both data spacing based on the lithological and the eU_3O_8 grade because their difference was not significant.

The software used for the simulation was Stanford Geostatistical Modeling Software (SGeMS) [17]. For further visualization, analysis, and block reporting, the Geovia Surpac program, licensed to PPGN-BATAN, was utilized. The number of realizations used in this research was 100 realizations.

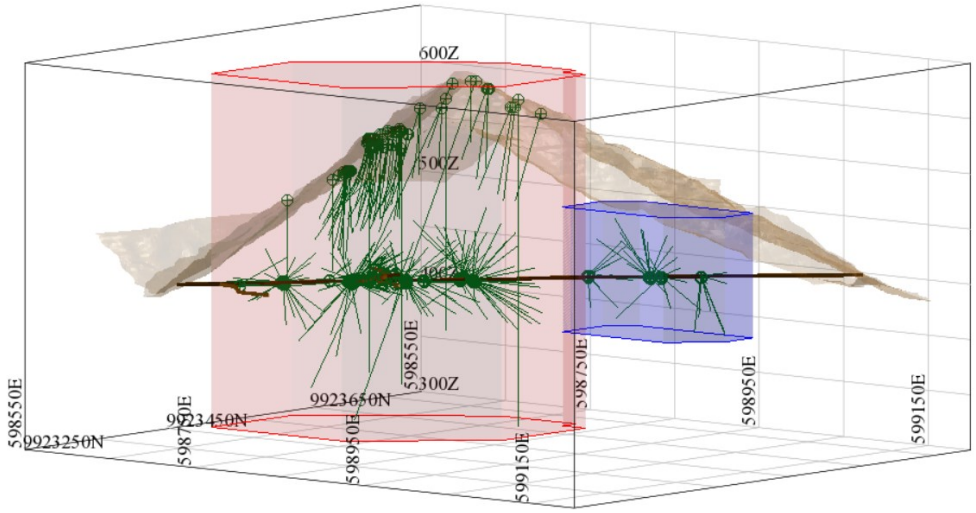

Figure 4. Distribution of drill hole data in 3D in a view perpendicular to the Eko-Remaja Tunnel (N340°E) which is divided into Block A (red area) and Block B (blue area).

Table 1. Statistical parameters, frequency, and global proportion of binary lithological data.

	Parameters	ML	MPS	MPJ	MA	MD	ZM	Total
Block A	Mean	0.477	0.247	0.031	0.023	0.012	0.182	
	Standard deviation	0.499	0.431	0.173	0.15	0.109	0.386	
	Variance	0.249	0.186	0.03	0.023	0.012	0.149	
	Frequency	7255	3759	465	348	184	3211	15221
	Global proportion	0.477	0.247	0.031	0.023	0.012	0.211	1
Block B	Mean	0.137	0.366	0.108	0.074	0.006	0.275	
	Standard deviation	0.343	0.482	0.31	0.261	0.075	0.447	
	Variance	0.118	0.232	0.096	0.068	0.006	0.2	
	Frequency	277	762	225	153	12	651	2080
	Global proportion	0.133	0.366	0.108	0.074	0.006	0.313	1

RESULTS

Variography Analysis

Based on structural geology data, the poles of lithological strike and dip were densely distributed around N290°E/66°, while the poles of strike and dip of uranium vein were distributed around N63°E/58° as can be seen in Figure 5. The first orientation was used for the experimental variogram construction of lithology 0, 1, and 3 of Block A, and the second orientation for lithology 5 of Block A. The orientation was used for the variogram experimental construction because it coincided with the anisotropy from the respective lithology. The variogram map is depicted in Figure 7. Other lithologies of

p-ISSN 0854-1418
e-ISSN 2503-426X

Block A used an omnidirectional experimental variogram. For Block B, an omnidirectional experimental variogram was used for all lithology because the structural data was taken only up to 200 meters from the Eko-Remaja tunnel's mouth. It was considered not representative of Block B which is located over 400 meters from the tunnel's mouth. The variogram model fitted from the experimental variogram used one or two structures of the spherical model, exponential model, or their combination. The variogram model of each lithology for Block A and Block B can be seen in Figure 8 and Figure 9, respectively, while the parameters can be seen in Table 2 and Table 3.

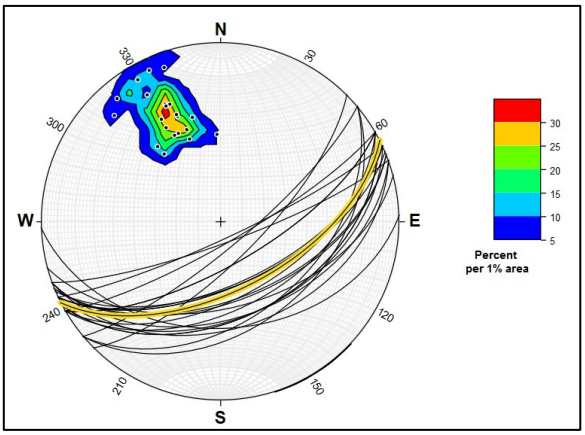

(A)

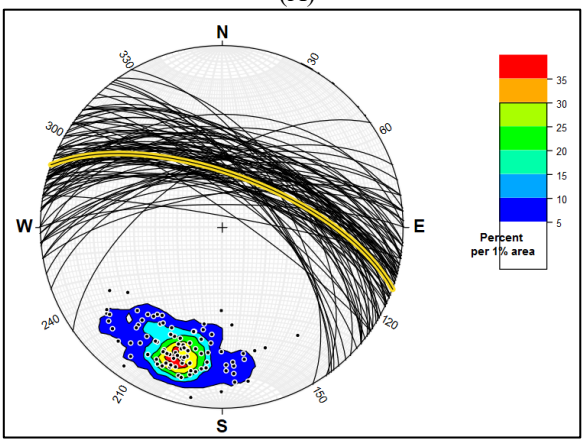

(B)

Figure 5. Contour analysis of the plane pole projection with the highest contour (arc with yellow outline) at N63°E/58° from metasediment layers (A) and N290°E/66° from U vein and mineralized breccia data (B)

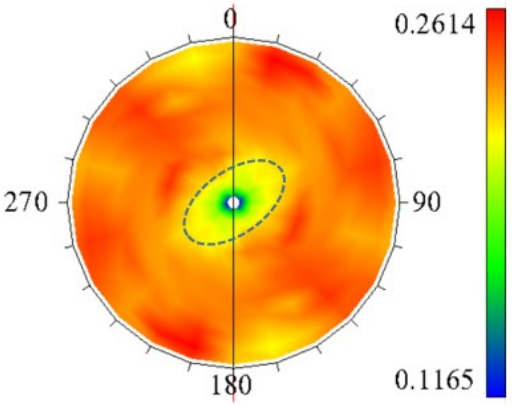

(A)

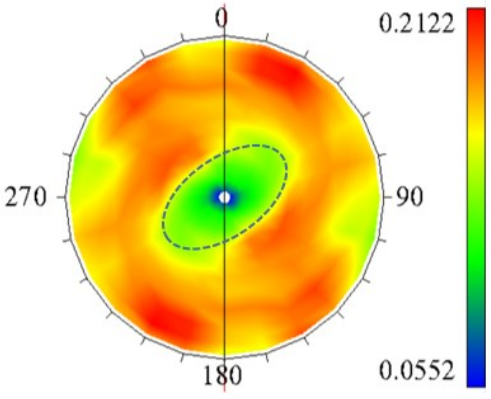

(B)

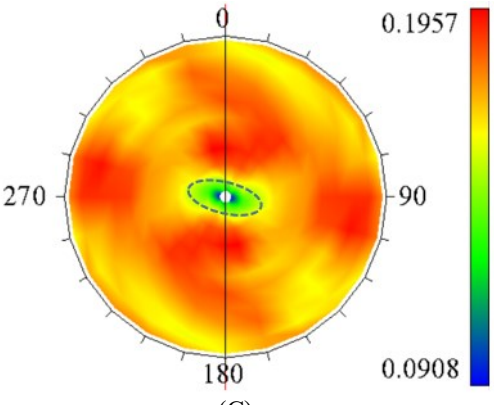

(C)

Figure 6. Variogram maps of binary lithology data of lithology 0 (A), 1 (B), and 5 (C)

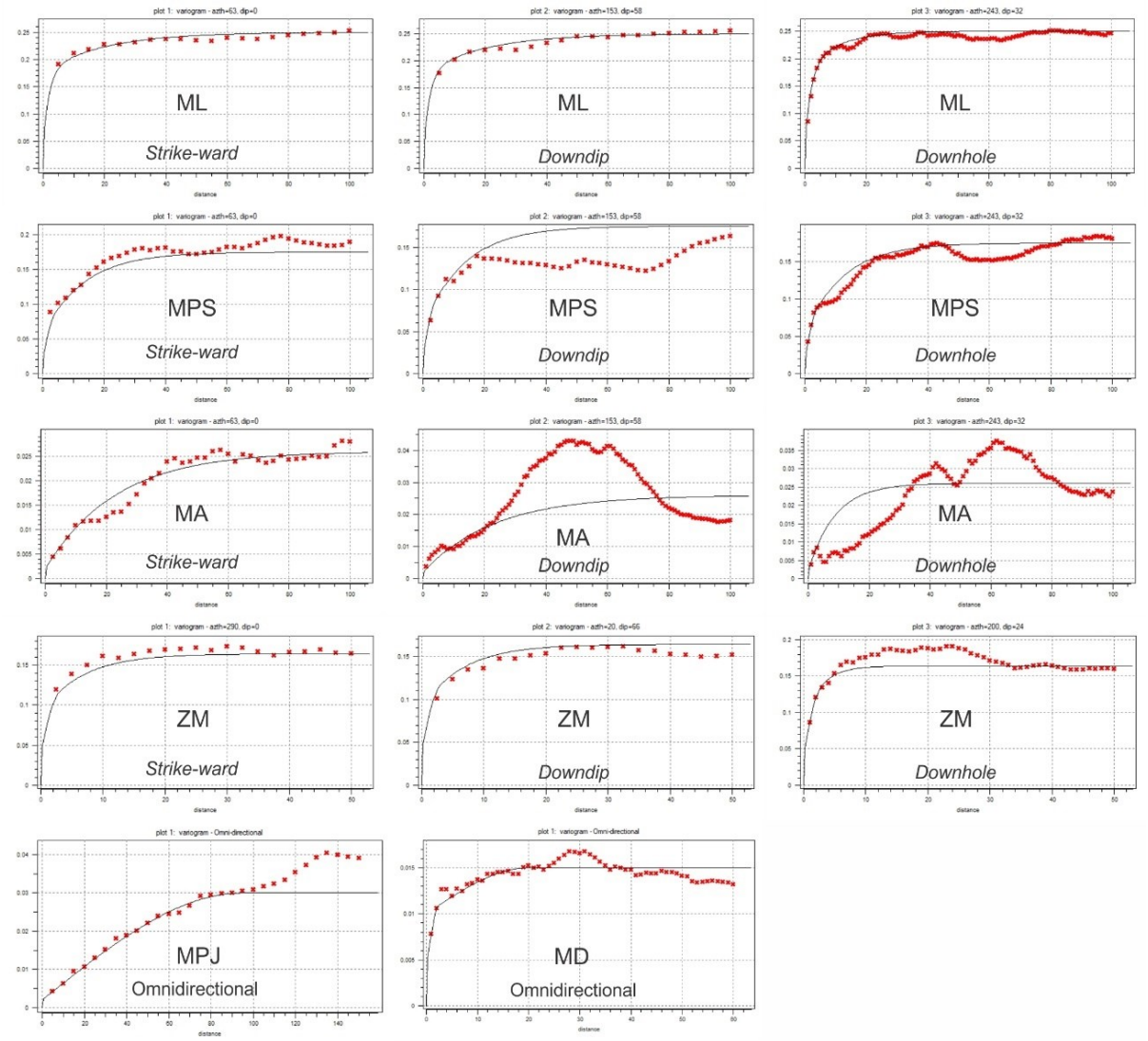

Figure 7. Variogram models of the lithology of Block A.

Table 2. Variogram model parameters of the lithology of Block A.

Lithological code	Variogram model									
	Nugget Effect	Sill		Range						
		C_1	C_2	a_1 max	a_1 med	a_1 min	a_2 max	a_2 med	a_2 min	
ML / 0	0.045	0.132	0.073	Theoretical model: Exponential			Theoretical model: Exponential			
				6	6	6	60	60	10	
MPS / 1	0.02	0.035	0.12	Theoretical model: Spherical			Theoretical model: Exponential			
				4	4	4	40	40	25	
MPJ / 2	0.002	0.028		Theoretical model: Spherical						
				95	95	95				
MA / 3	0.002	0.024		Theoretical model: Exponential						
				70	70	8				
MD / 4	0.004	0.006	0.005	Theoretical model: Spherical			Theoretical model: Spherical			
				2	2	2	20	20	20	
ZM / 5	0.04	0.05	0.074	Theoretical model: Spherical			Theoretical model: Exponential			
				3	3	3	20	20	8	

p-ISSN 0854-1418
e-ISSN 2503-426X

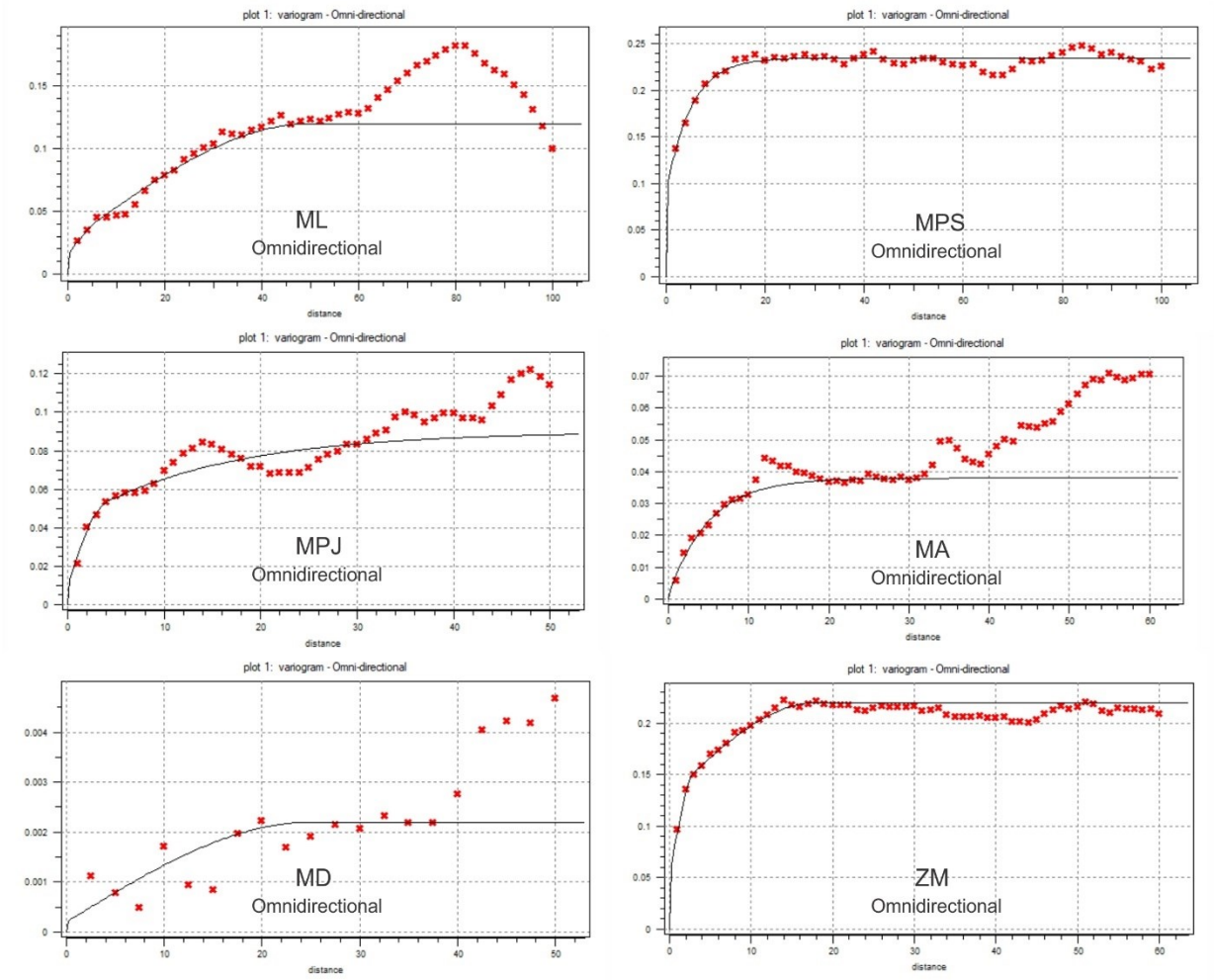

Figure 8. Variogram models of the lithology of Block B.

Table 3. Variogram model parameters of the lithology of Block B.

Lithological code	Variogram model								
	Nugget Effect	Sill		Range					
		C_1	C_2	a_1 max	a_1 med	a_1 min	a_2 max	a_2 med	a_2 min
ML / 0	0.015	0.01	0.095	Theoretical model: Spherical			Theoretical model: Spherical		
				6	6	6	60	60	6
MPS / 1	0.09	0.145		Theoretical model: Spherical					
				15	15	15			
MPJ / 2	0.01	0.032	0.048	Theoretical model: Spherical			Theoretical model: Exponential		
				4	4	4	45	45	45
MA / 3	0.001	0.037		Theoretical model: Spherical					
				15	15	15			
MD / 4	0.002	0.002		Theoretical model: Spherical					
				25	25	25			
ZM / 5	0.05	0.08	0.09	Theoretical model: Spherical			Theoretical model: Spherical		
				3	3	3	18	18	18

Simulation Result and Validation

The SIS simulation resulted in a series of 100 lithological numerical values in each block cell called the realization. The first validation was the lithological values histogram comparison between the input and the realization [34]. Three realizations that were selected randomly and compared to the input were displayed in Figure 9. The histograms showed a strong resemblance between respective input and output. It validated that the SIS simulation has been done properly.

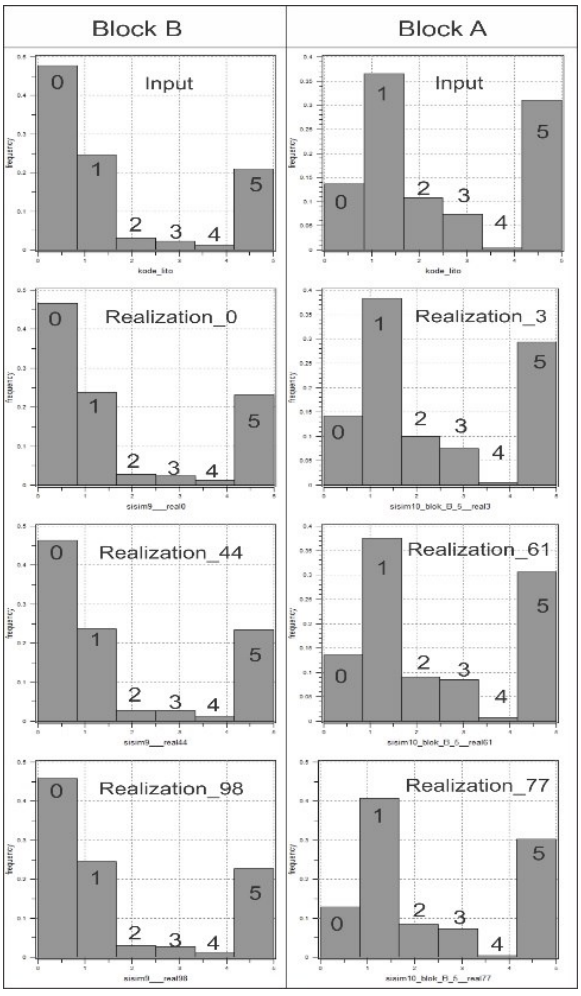

Figure 9. Histogram comparison between input and three selected realizations of Block A and Block B.

From the 100 values, the probability of each lithology in each block cell was determined. The lithology with maximum probability was assigned to represent the block's lithology. The block model was then validated visually with the geological map of the Eko-Remaja Tunnel at level 450 masl at the 450 masl section of the model, as can be seen in Figure 10 for Block A and Block B. The comparison between the model and map indicated general similar nature of lithology distribution and the lithology along the tunnel that was mapped directly. It concluded that the model was well validated visually with the map so it could be used for further analysis.

To increase confidence in the validity of the simulation results, a comparison of the simulated blocks with lithology along the borehole was also carried out. The percentage of suitability was calculated according to the matched block lithology compared to the borehole lithology. Figure 11 shows a comparison of the suitability of the simulated block with the lithology along drill hole TL-111 as an example. Meanwhile, the percentage of the suitability of the simulated block with three lithologies from randomly selected drill holes was presented in Table 4. In both Block A and Block B, the percentage of the suitability of the simulated block with the lithology of the borehole shows a high value. This result strengthened the validation that the simulation has been carried out well.

p-ISSN 0854-1418
e-ISSN 2503-426X

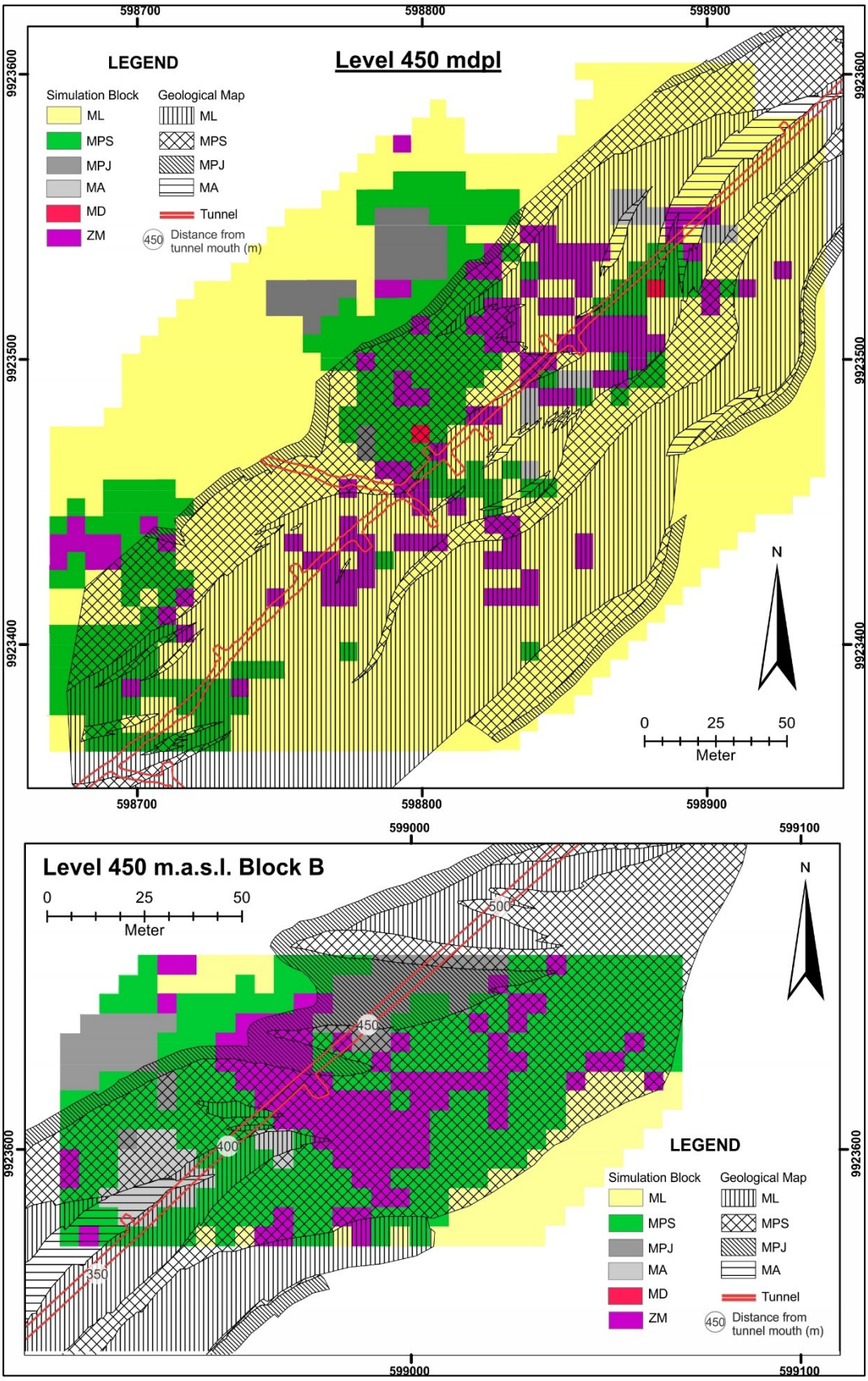

Figure 10. Comparison between geostatistical SIS model and geological map of Eko-Remaja Tunnel level 450 masl on Block A and Block B.

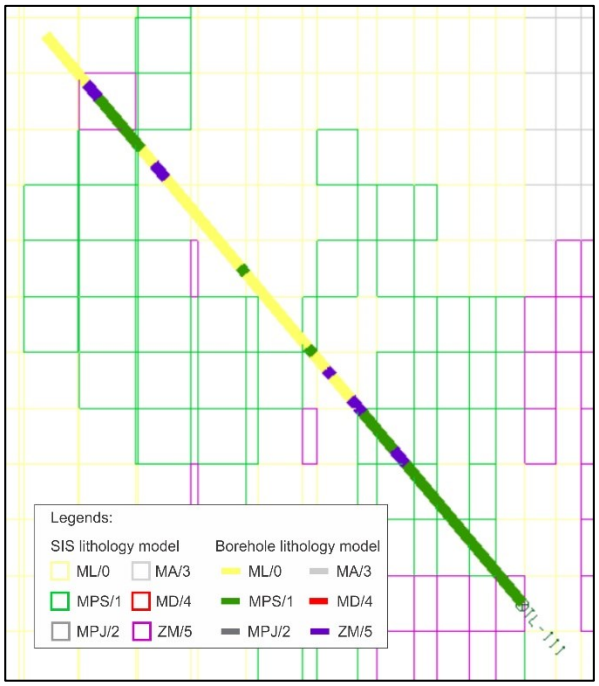

Figure 11. Example of a comparison of the suitability of SIS simulation lithology with lithology along borehole TL-111.

Table 4. Comparison of the suitability of SIS and manual ore body models to three randomly selected borehole lithology.

	Borehole code	Percentage of Suitability of SIS simulation lithology with lithology along the borehole (%)
Block A	TL-177	87,2
	TL-222	76,9
	TL-165	73,3
	Average	**79,1**
Block B	TL-156	93,3
	TL-111	90,0
	EFKL-09	100,0
	Average	**94.4**

Geostatistical SIS Ore Body Model

For the geostatistical SIS models, the minimum probability of 0.5 of mineralization zone (ZM) lithology with numerical code 5 was defined as ore body. The ore body models are pictured from some points of view in Figure 12 and Figure 13 for Block A and Block B, respectively. The model showed E-W tabular geometry. It appeared dipping relatively to the north, although it was only better observed in Block B.

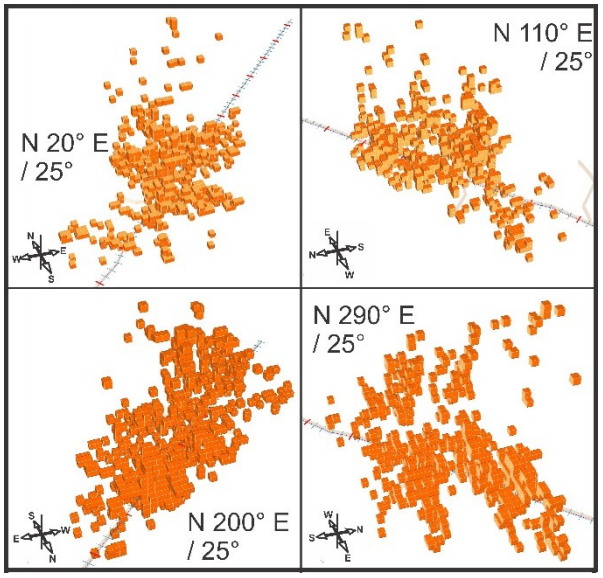

Figure 12. Geostatistical SIS models of Block A from some points of view.

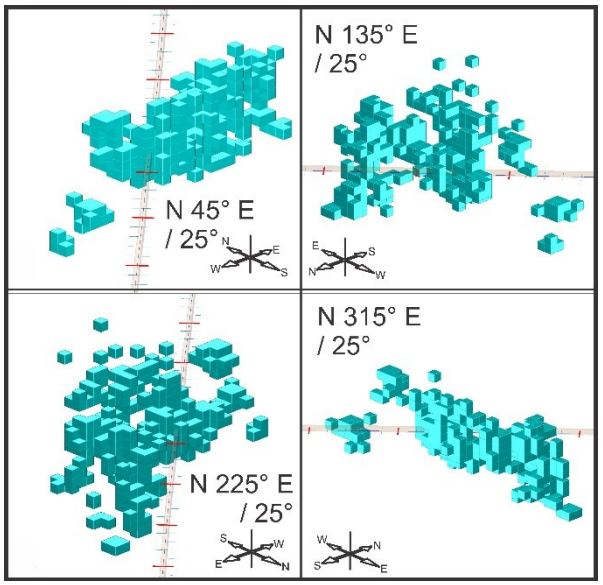

Figure 13. Geostatistical SIS models of Block B from some points of view.

DISCUSSION

Visual & Descriptive Comparative Analysis

The visual comparison between the geostatistical SIS and the manual ore body model was depicted in Figure 14 for Block A and Figure 15 for Block B. The difference in the dimension of the two model types was visible. However, the distribution of the ore bodies was quite spatially corresponded, especially near tunnels that have a large data

p-ISSN 0854-1418
e-ISSN 2503-426X

density. Most of the manual models were also observed to coincide with or penetrate the SIS block model. Manual ore bodies were constructed based on thin vein geometries and were not correlated to a single zone, resulting in individual ore bodies. Meanwhile, in the SIS block model, the database accommodated the correlated mineralized zones. This caused the block model distribution to look like a mineralized zone extension of the manual model.

Regardless of the spatial suitability based on visual comparisons of the two types of models, both types of models still have advantages and disadvantages. These advantages and disadvantages can be taken into consideration when choosing a model as the grade estimation domain. The comparison of the two models can be seen in Table 5.

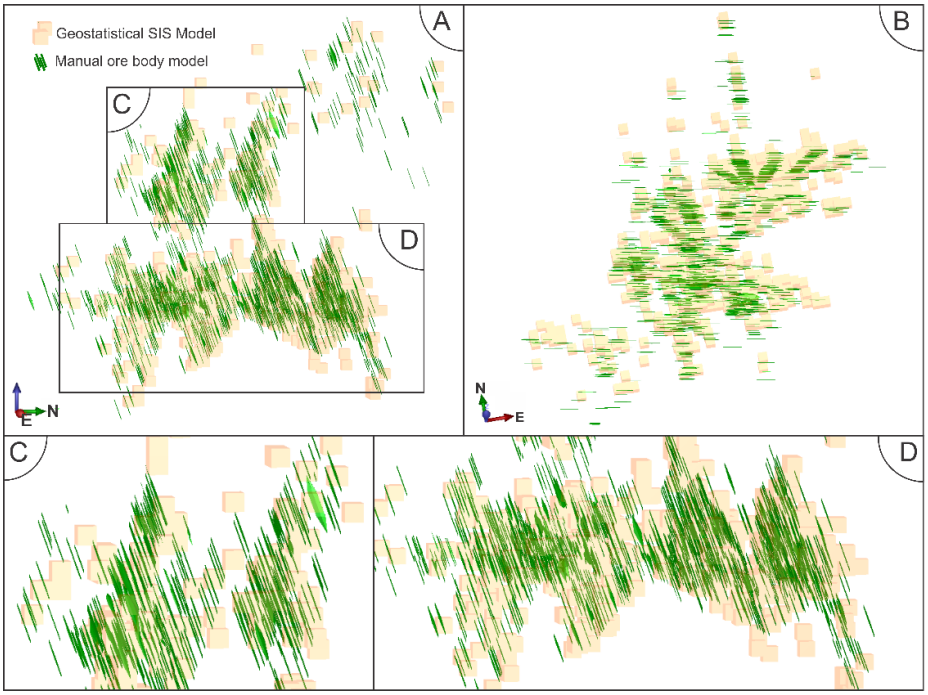

Figure 14. Comparison between geostatistical SIS model and manual ore body models of Block A at manual ore body's strike-ward point of view (A) and downdip (B).

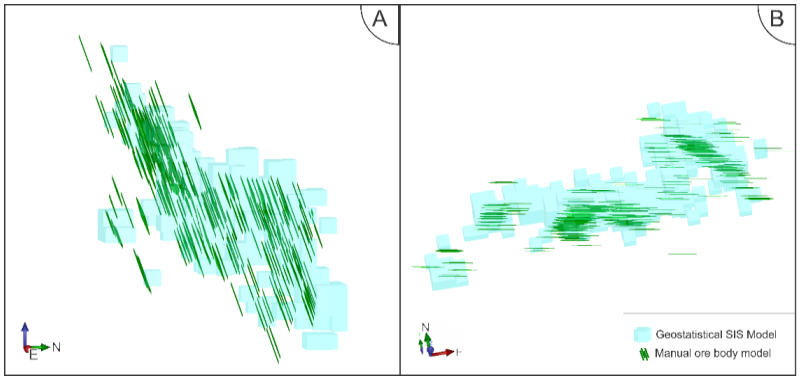

Figure 15. Comparison between geostatistical SIS model and manual ore body models of Block B at manual ore body's strike-ward point of view (A) and downdip (B).

Table 5. A descriptive comparison of manual and geostatistical ore body models of SIS in the Remaja Sector

Manual ore body model	Geostatistical ore body model
Created directly by humans based on the interpretation of field data.	Created with the help of the program, the result depends on the input entered in the simulation.
Long processing time.	Processing time was relatively faster.
Due to data limitations, assumptions were used in determining vein continuity.	Determination of continuity based on variogram parameters and searching ellipsoid.
Not equipped with uncertainty properties such as probability. Each resulting solid model was considered an ore body based on the assumptions.	Equipped with an uncertainty factor in the form of the probability of the ore body.
Modeled in a solid format with a thin geometry. If a block model is to be made for grade estimation, the dimension of the block that corresponds to the spacing between grade data will be greater than the thickness of the solid model. It will increase geological uncertainty.	Modeled in a block model format, so the suitability of the geometry in the field is limited to the shape and size of the block. On the other hand, the block size has been adjusted according to the distance between grade data so that grade uncertainty has been reduced.
The vein continuity is modeled by considering the presence of other lithologies but does not differentiate these lithologies. Its suitability to actual geological conditions can only be validated against the presence of ore bodies along the tunnel wall.	The simulation process considers the existence of other lithologies and their types so that it can be seen their suitability to actual geological conditions, both the suitability of the ore body and other lithologies.

Quantitative Comparative Analysis

To see the quantitative comparison of suitability between the two models, the percentage of conformity of the two models to the lithology of a borehole was used. It was done by counting the numbers of blocks along the drill holes that were suitable and not, compared to the lithology of the mineralized zone in the drill hole (ZM/5). Then, the corresponding SIS geostatistical ore body block percentage was calculated. This comparison did not look at other lithological suitability lithologies other than the mineralized zone (ZM/5). The same method was applied to manual ore body models that penetrate boreholes. The manual ore body model that was suitable or not with the lithology of the mineralized zone was counted (ZM/5) so that the percentage of the appropriate manual ore body model can be determined. This process was carried out on five randomly selected drill holes, both in Block A and Block B. For example, Figure 16 presents a comparison of the suitability of the SIS and manual ore body models to the lithology of drill hole EFKL-02.

Meanwhile, the comparison of the suitability of the SIS and manual geostatistical ore body models to the lithology of five randomly selected drill holes can be seen in Table 6. In general, for each borehole, the percentage fit of the SIS and manual geostatistical ore body models varies. There were some percentages of the suitability of the SIS geostatistical ore body model which is superior to the manual ore body model in several drill holes, but there were also smaller percentages of conformity to the SIS geostatistical ore body model compared to the manual ore body model. However, the average percentage suitability value shows that the SIS geostatistical ore body model is higher than the manual ore body model in both Block A and Block B.

p-ISSN 0854-1418
e-ISSN 2503-426X

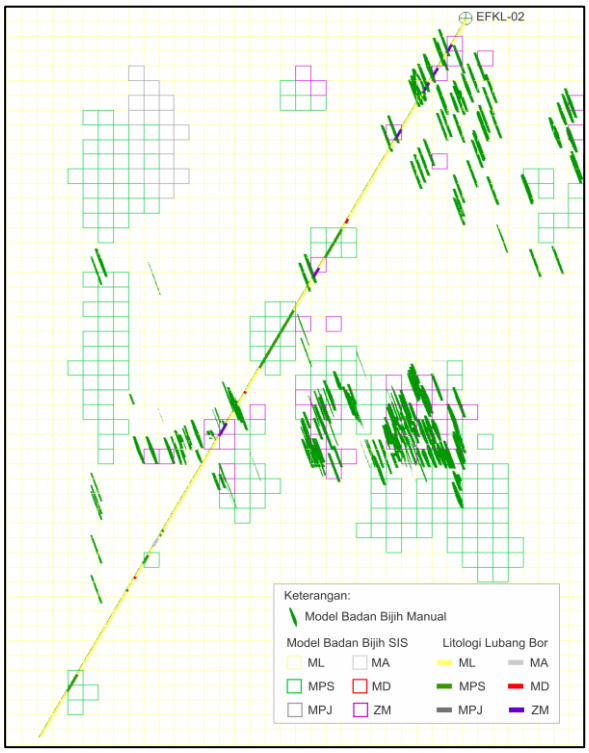

Figure 16. Example of comparison of the suitability of SIS and manual ore body models to borehole lithology EFKL-02

Table 6. Comparison of the suitability of SIS and manual ore body models to randomly selected borehole lithology

	Borehole code	Percentage of Suitability of Ore Body Model to Borehole Lithology (%)	
		SIS	Manual
Block A	EFKL-02	71,4	46,2
	TL-096	61,5	33,3
	EFKL-03	60,0	33,3
	TL-115	66,7	66,7
	TL-073	61,5	61,5
	Average	**64,2**	**48,2**
Block B	TL-207	75,0	55,6
	TL-169	60,0	70,0
	TL-205	57,1	47,1
	TL-173	80,0	14,3
	TL-225	77,8	62,5
	Average	**70,0**	**49,9**

Probability-Volume Sensitivity Analysis

The probability analysis of 0.5 was the minimum probability for a block to be classified as an ore body. The higher probability above 0.5 had a better degree of confidence as it spatially included more data in the simulation. Lithological probability could be used in some cut-offs above 0.5 as a tool to indicate the different degrees of confidence. This practically affects the volume of the ore body. Figure 17 demonstrated the change in volume of the ore body (block size of 6×6×6 m^3 for Block A and a block size of 5×5× m^3 for Block B) as different probability cut-offs were applied.

Based on Figure 17, as the higher lithological probability cut-off was applied (i.e. 0.7 and 0.9), the ore body volume decreased. On Block A, over 20% of volume decreased from the block model with a probability cut-off of 0.5 to 0.7. On Block B, the volume decreased by over 50%. In contrast, the changing in volume from the block model with a probability cut-off of 0.7 to 0.9 were low, both in Block A and Block B.

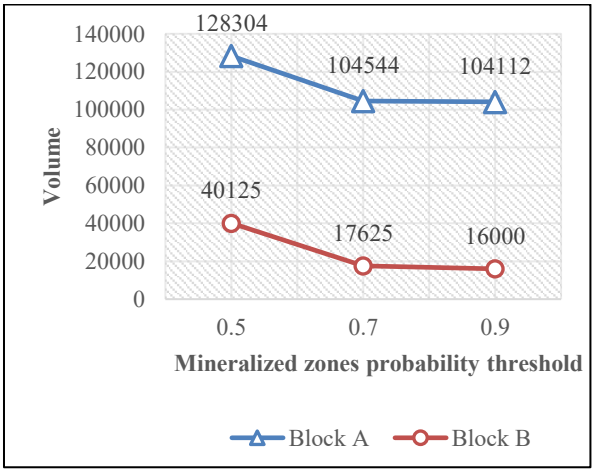

Figure 17. Block model volume according to different mineralized zones' probability thresholds

CONCLUSIONS

Based on the comparative analysis, the geostatistical and manual ore body models in the Remaja Sector have their respective strengths and weaknesses. The weakness of

the geostatistical ore body model is that the results depend on the input parameters in the simulation which are considered inferior to the manual model guided by the interpretation of field data. Meanwhile, the geostatistical ore body model has the advantage of being faster in processing, equipped with an uncertainty factor, and the block size of the model has taken into account the distance between grade data so that it can be used directly for grade estimation. Quantitatively, the geostatistical ore body model has a higher average percentage of conformity to the lithology of the mineralized zone along the borehole than the manual ore body model. Therefore, the geostatistical ore body model was used as the limit in grade estimation in the Remaja Sector. The SIS geostatistical ore body model had a volume of about 128,000 m^3 and 40,000 m^3 respectively for Block A and Block B. As the higher lithological probability was applied (i.e. 0.7 and 0.9), the volume decreased by over 20% and 50% respectively for Block A and Block B.

ACKNOWLEDGMENT

The authors would like to express gratitude to Dr. Syaiful Bakhri as the Head of the Research Center for Nuclear Fuel Cycle and Radioactive Waste Technology for the topic and data usage permission for this research. The authors are also deeply thankful to Mr. Suharji who initially build the Remaja Sector database, taught the authors about the software operation, guided the authors on the manual ore body modeling, and also gave comprehensive geological knowledge of the Remaja Sector in the field to the authors. The work presented in this paper was supported by the Science and Technology Scholarship as stated in the Decision of The National Research and Innovation Agency Deputy Chairman for Human Resource of Science and Technology Issue 2/II/HK/2022 about Civil Servants Recipient of National Research and Innovation Agency Scholarship Continuation.

AUTHOR CONTRIBUTIONS

RCC and MNH are the main contributors while HS, DK, and PR are the member contributors. RCC, MNH, and HS designed this study; RCC, DK, and PR built the database and worked on the manual ore body modeling; RCC and MNH performed the data and variogram analysis, also the geostatistical simulation and the comparison between the models; RCC wrote the manuscript; MNH and HS revised the manuscript. All authors read and approved the final manuscript.

REFERENCES

[1] S. Tjokrokardono, "Prospek Pengembangan Cebakan Uranium di Kalan, Kalimantan," *J. Nukl. Indones.*, vol. 1, no. 1, pp. 1–12, 1998.

[2] S. Tjokrokardono, D. Soetarno, M. Sapardi, L. Subiantoro, and R. Witjahyati, "Studi Geologi Regional dan Mineralisasi Uranium di Pegunungan Schwaner Kalimantan Barat dan Tengah," in *Prosiding Seminar Geologi Nuklir dan Sumber Daya Tambang*, 2004, pp. 64–84.

[3] BATAN-CEA, "Prospect to Develop Uranium Deposits in Kalimantan Volume I and II, Introduction to General Reconnaissance," Jakarta, 1977.

[4] H. Syaeful, F. D. Indrastomo, and M. B. Garwan, "Application of UNFC for the reassessment of uranium resources of the Eko Remaja and Rabau Sectors, Kalan Area, West Kalimantan, Indonesia," in *UNECE Energy Series 58 Application of the United Nations Framework Classification for Resources: Case Study*, Geneva: United Nation Publication, 2019, pp. 137–147.

[5] R. Ciputra, S. Suharji, D. Kamajati, and H. Syaeful, "Application of geostatistics to complete uranium resources estimation of Rabau Hulu Sector, Kalan, West Kalimantan," *E3S Web Conf.*, vol. 200, 2020.

[6] H. Syaeful and Suharji, "Eksplorium Geostatistics Application on Uranium Resources Classification : Case Study of Rabau Hulu Sector , Kalan , West Kalimantan Aplikasi Geostatistik pada Klasifikasi Sumber Daya Uranium : Studi Kasus," *Eksplorium*, vol. 39, no. 2, pp. 131–140,

2018.
[7] H. Syaeful, Suharji, and A. Sumaryanto, "Pemodelan Geologi dan Estimasi Sumber Daya Uranium di Sektor Lemajung, Kalan, Kalimantan Barat," in *Prosiding Seminar Nasional Teknologi Energi Nuklir*, 2014, pp. 329–342.
[8] E. Cowan *et al.*, "Practical Implicit Geological Modelling," in *5th International Mining Geology Conference*, 2003, pp. 89–99.
[9] M. Abzalov, *Applied Mining Geology, Modern Approach in Solid Earth Sciences 12*. Switzerland: Springer, 2016.
[10] M. E. Rossi and C. V. Deutsch, *Mineral Resource Estimation*. New York: Springer, 2014.
[11] K. Novak-Zelenika, "Theory of deterministical and stochastical indicator mapping methods and their applications in reservoir characterization, a case study of the Upper Miocene reservoir in the Sava Depression," *Rud. Geol. Naft. Zb.*, vol. 32, no. 3, pp. 45–53, 2017.
[12] M. Maleki, X. Emery, and N. Mery, "Indicator variograms as an aid for geological interpretation and modeling of ore deposits," *Minerals*, vol. 7, no. 12, 2017.
[13] Y. He *et al.*, "Sequential indicator simulation and indicator kriging estimation of 3-dimensional soil textures," *Aust. J. Soil Res.*, vol. 47, no. 6, pp. 622–631, 2009.
[14] H. Talebi, O. Asghari, and X. Emery, "Stochastic rock type modeling in a porphyry copper deposit and its application to copper grade evaluation," *J. Geochemical Explor.*, vol. 157, pp. 162–168, 2015.
[15] R. Gutierrez and J. Ortiz, "Sequential Indicator Simulation with Locally Varying Anisotropy – Simulating Mineralized Units in a Porphyry Copper Deposit.," *J. Min. Eng. Res.*, vol. 1, no. 1, pp. 1–7, 2019.
[16] O. Asghari, "Geostatistical simulation of dyke systems in Sungun porphyry copper deposit, Iran," *J. Min. Environ.*, vol. 6, no. 1, pp. 1–10, 2015.
[17] N. Remy, A. Boucher, and J. Wu, *Applied Geostatistics with SGeMS: A user's guide*, vol. 9780521514. 2009.
[18] J. J. Gómez-Hernández and R. M. Srivastava, "One Step at a Time: The Origins of Sequential Simulation and Beyond," *Math. Geosci.*, vol. 53, no. 2, pp. 193–209, 2021.
[19] F. Zhou, D. Shields, S. Tyson, and J. Esterle, "Comparison of sequential indicator simulation, object modeling and multiple-point statistics in reproducing channel geometries and continuity in 2D with two different spaced conditional datasets," *J. Pet. Sci. Eng.*, vol. 166, no. February 2016, pp. 718–730, 2018.
[20] Y. Liu, Q. Xia, and E. J. M. Carranza, "Integrating sequential indicator simulation and singularity analysis to analyze the uncertainty of geochemical anomaly for exploration targeting of tungsten polymetallic mineralization, Nanling belt, South China," *J. Geochemical Explor.*, vol. 197, no. July 2018, pp. 143–158, 2019.
[21] M. Tokoglu, "Comparative Analysis of 3D Domain Modelling Alternatives: Implications for Mineral Resource Estimates," Colorado School of Mines, 2018.
[22] F. G. Bastante, C. Ordóñez, J. Taboada, and J. M. Matías, "Comparison of indicator kriging , conditional indicator simulation and multiple-point statistics used to model slate deposits," *Eng. Geol.*, vol. 98, pp. 50–59, 2008.
[23] A. I. Xiao, S. Baitao, and C. Xiangzhao, "Integrated 3d modeling of quaternary sediments in the Beijing plain, based on a sequential indicator simulation," *Geol. Croat.*, vol. 72, no. Special Issue, pp. 3–17, 2019.
[24] S. Hajsadeghi, O. Asghari, M. Mirmohammadi, and S. A. Meshkani, "Indirect rock type modeling using geostatistical simulation of independent components in Nohkouhi volcanogenic massive sulfide deposit, Iran," *J. Geochemical Explor.*, vol. 168, pp. 137–149, 2016.
[25] H. T. Breitfeld *et al.*, "Mesozoic Paleo-Pacific Subduction Beneath SW Borneo: U-Pb Geochronology of the Schwaner Granitoids and the Pinoh Metamorphic Group," *Front. Earth Sci.*, vol. 8, no. December 2020.
[26] J. Hennig, H. T. Breitfeld, R. Hall, and A. M. S. Nugraha, "The Mesozoic tectono-magmatic evolution at the Paleo-Pacific subduction zone in West Borneo," *Gondwana Res.*, vol. 48, pp. 292–310, 2017.
[27] L. Davies, R. Hall, and R. Armstrong, "Cretaceous Crust in South West Borneo: Petrological, Geochemical, and Geochronological Constraints from the Schwaner Mountains," in *Proceedings Indonesian Petroleum Association 38th Annual Convention & Exhibition*, 2014.
[28] H. S. Karyono, "Temperatur Pembentukan Vein Mineralisasi di Bukit Eko, Kalan, Kalimantan Barat," in *Proceedings of The Indonesian Association of Geologist XXI Annual Scientific Meeting*, 1992, p. 281.
[29] H. S. Karyono, "Analisis Kontrol Tektonik pada Vein Mineralisasi di Bukit Eko, Kalan, Kalimantan Barat," in *Proceedings of The Indonesian Association of Geologist XX Annual Scientific Meeting*, 1991, pp. 115–128.
[30] A. G. Muhammad, R. C. Ciputra, and H. Syaeful, "Fracture Analysis of Uranium-Bearing Rock in Eko-Remaja Exploration Tunnel at Depth 50-200 Meters, Kalan, West Kalimantan," *J. Phys. Conf. Ser.*, vol. 1363, no. 1, 2019.
[31] H. S. Karyono, "Typolohie des structures mineralisees du bassin de la Kalan, Kalimantan

de L'Ouest, Indonesia: Aspect tectonique et controle structural des mineralisations d'uranium," L'Universute Louis Oasteur, 1989.

[32] R. C. Ciputra, A. G. Muhammad, and T. B. Adimedha, "Estimasi Sumber Daya Uranium Tipe Batupasir di Sektor Aloban , Sibolga , Tapanuli Tengah Uranium Resources Estimation of Sandstone-Type Deposit in Aloban Sector ," *Eksplorium*, vol. 40, no. 1, pp. 1–10, 2019.

[33] D. Soetarno, "Geokronologi U-Pb pada Mineralisasi Uranium di Eko dan Rirang, Kalan, Kalimantan Barat," in *Proceedings of The Indonesian Association of Geologist XXI Annual Scientific Meeting*, 1992, pp. 257–264.

[34] A. Ersoy and T. Y. Yünsel, "The assessment of soil contamination by heavy metals using geostatistical sequential Gaussian simulation method," *Hum. Ecol. Risk Assess.*, vol. 24, no. 8, pp. 2142–2161, 2018.